Applied Physics Letters

Record >10 MV/cm mesa breakdown fields in $Al_{0.85}Ga_{0.15}N/Al_{0.6}Ga_{0.4}N$ high electron mobility transistors on native AlN substrates

Cite as: Appl. Phys. Lett. **120**, 172106 (2022); https://doi.org/10.1063/5.0083966
Submitted: 31 December 2021 • Accepted: 18 April 2022 • Published Online: 26 April 2022

Dolar Khachariya, Seiji Mita, Pramod Reddy, et al.

Applied Physics Letters ARTICLE scitation.org/journal/apl

Record >10 MV/cm mesa breakdown fields in $Al_{0.85}Ga_{0.15}N/Al_{0.6}Ga_{0.4}N$ high electron mobility transistors on native AlN substrates

Cite as: Appl. Phys. Lett. **120**, 172106 (2022); doi: 10.1063/5.0083966
Submitted: 31 December 2021 · Accepted: 18 April 2022 ·
Published Online: 26 April 2022

View Online Export Citation CrossMark

Dolar Khachariya,[1] Seiji Mita,[2] Pramod Reddy,[2] Saroj Dangi,[1] J. Houston Dycus,[3] Pegah Bagheri,[4] M. Hayden Breckenridge,[4] Rohan Sengupta,[1] Shashwat Rathkanthiwar,[4] Ronny Kirste,[2] Erhard Kohn,[4] Zlatko Sitar,[2,4] Ramón Collazo,[4] and Spyridon Pavlidis[1,a)]

AFFILIATIONS

[1]Department of Electrical and Computer Engineering, North Carolina State University, Raleigh, North Carolina 27695-7911, USA
[2]Adroit Materials, Inc., 2054 Kildaire Farm Rd., Cary, North Carolina 27518, USA
[3]EAG Eurofins Materials Science, Raleigh, North Carolina 27606, USA
[4]Department of Materials Science and Engineering, North Carolina State University, Raleigh, North Carolina 27695-7919, USA

Note: This paper is part of the APL Special Collection on Wide- and Ultrawide-Bandgap Electronic Semiconductor Devices.
[a)]**Author to whom correspondence should be addressed:** spavlidis@ncsu.edu

ABSTRACT

The ultra-wide bandgap of Al-rich AlGaN is expected to support a significantly larger breakdown field compared to GaN, but the reported performance thus far has been limited by the use of foreign substrates. In this Letter, the material and electrical properties of $Al_{0.85}Ga_{0.15}N/Al_{0.6}Ga_{0.4}N$ high electron mobility transistors (HEMT) grown on a 2-in. single crystal AlN substrate are investigated, and it is demonstrated that native AlN substrates unlock the potential for Al-rich AlGaN to sustain large fields in such devices. We further study how Ohmic contacts made directly to a Si-doped channel layer reduce the knee voltage and increase the output current density. High-quality AlGaN growth is confirmed via scanning transmission electron microscopy, which also reveals the absence of metal penetration at the Ohmic contact interface and is in contrast to established GaN HEMT technology. Two-terminal mesa breakdown characteristics with 1.3 μm separation possess a record-high breakdown field strength of ~11.5 MV/cm for an undoped $Al_{0.6}Ga_{0.4}N$-channel layer. The breakdown voltages for three-terminal devices measured with gate-drain distances of 4 and 9 μm are 850 and 1500 V, respectively.

GaN channel high electron mobility transistors (HEMTs) have become exciting candidates for high-frequency and high-power switching applications.[1–4] With the ever-present demand for higher performance, ultra-wide bandgap (UWBG) semiconductors are gaining attention as next-generation high-power and high-frequency electronics due to their higher breakdown fields and capability to operate at higher temperatures.[5] In particular, Al-rich AlGaN-based transistors possess large Johnson's and Baliga's figures of merit[6,7] due to their large critical electric field (E_C), which increases rapidly from ~3.7 MV/cm for GaN to ~17 MV/cm for AlN.[8,9]

Most Al-rich AlGaN-based transistors are grown on sapphire substrates with AlN templates.[10–12] The larger dislocation density in such films limits the E_C. For example, Abid *et al.* measured a breakdown field of ~6 MV/cm between isolated contacts in the AlN buffer layer grown on sapphire substrates.[11,12] While relatively high, the reported E-field is low compared to the ideal E_C for AlN. In this work, we report a record high breakdown field of ~11.5 MV/cm in the $Al_{0.6}Ga_{0.4}N$ layer measured via mesa isolation structures between $Al_{0.85}Ga_{0.15}N/Al_{0.6}Ga_{0.4}N$ heterojunctions grown on native AlN substrates. These results underscore the potential of Al-rich AlGaN when state-of-the-art quality epilayers (TDD < 10^3 cm^{-2}) are used.[13–15] We also study the impact of the Ohmic contact layout on the knee voltage and current density when the top of the channel layer is Si-doped. We recently reported preliminary results for this structure.[16] In this Letter, we expand on this: we analyze the voltage dependence of the mesa breakdown I–V characteristics, report three-terminal breakdown characteristics for the HEMTs, and further analyze $Al_{0.85}Ga_{0.15}N/Al_{0.6}Ga_{0.4}N$ heterojunctions via C–V. Moreover, we demonstrate the high-quality growth of these structures on native AlN substrates via transmission electron microscopy (TEM) analysis.

AlGaN-channel HEMT epilayers were grown using a vertical, cold-wall, radio frequency (RF) heated, low-pressure metalorganic chemical vapor deposition (MOCVD) system on 2-in. diameter (0001)-plane single crystal, PVT AlN substrates with dislocation density $<10^3\,cm^{-2}$. The HEMT structure consists, bottom to top, of a 500 nm unintentionally doped (UID) AlN layer, a 300 nm of $Al_{0.6}Ga_{0.4}N$ channel layer, and a 20 nm of $Al_{0.85}Ga_{0.15}N$ barrier layer [Fig. 1(a)]. The upper half (150 nm) of the $Al_{0.6}Ga_{0.4}N$ channel layer is doped with Si at $5 \times 10^{17}\,cm^{-3}$. The reason for introducing doping in the channel layer instead of the barrier layer[10] is to avoid high gate leakage. This also allows Ohmic contacts to be made directly to the doped channel layer, as discussed below. The RMS roughness of the HEMT structure after the growth is around 0.5 nm.

Device fabrication started with a 230 nm deep mesa etch with a 12° bevel sidewall, confirmed via AFM. V/Al/Ni/Au (30/100/70/70 nm) were deposited via e-beam evaporation for the source (S) and drain (D) contacts. Two types of S/D contact geometries were realized: (1) S/D contacts only on top of the mesa (device-A) [Fig. 1(b)] and (2) S/D contacts extended over the beveled mesa sidewall (device-B) [Fig. 1(c)]. The S/D contacts were then annealed at 950 °C for 60 s in N_2 ambient. Gates were formed via e-beam evaporation of Ni/Au contacts. SEM images of device-A and device-B post-fabrication are shown in Figs. 1(d) and 1(e), respectively. It should be noted that these HEMTs are unpassivated.

Figure 1(f) shows the temperature-dependent Hall measurements performed via the van der Pauw method. A sheet carrier density (n_S) of $\sim 1.9 \times 10^{13}\,cm^{-2}$, a mobility ($\mu_n$) of $140\,cm^2/V\,s$, and a sheet resistance (R_{SH}) of 2500 $\Omega/\square$ are measured at room temperature. It should be noted that n_S is the total density from the two-dimensional electron gas (2DEG) region and a 150 nm n-type doped $Al_{0.6}Ga_{0.4}N$ channel. The experimentally measured sheet carrier density is in agreement with the simulated sheet carrier density via a BandEng simulator.[17] At temperatures lower than 200 K, temperature-independent n_S and μ_n are observed, confirming the 2DEG's presence. At 90 K, $n_S \sim 1.7 \times 10^{13}\,cm^{-2}$, and $\mu_n \sim 200\,cm^2/V\,s$. From room temperature to high temperature, an exponential rise in n_S and a reduction in μ_n are observed due to the activation of carriers in the Si-doped n-type $Al_{0.6}Ga_{0.4}N$ channel. At 750 K, $n_S \sim 3.9 \times 10^{13}\,cm^{-2}$, and $\mu_n \sim 30\,cm^2/V\,s$. The same structure grown on a sapphire substrate (dislocation density $\sim 10^{10}\,cm^{-2}$) shows $n_S \sim 7.6 \times 10^{12}\,cm^{-2}$, $\mu_n \sim 92\,cm^2/V\,s$, and $R_{SH} \sim 8900\ \Omega/\square$ at room temperature. Thus, the HEMT on the AlN substrate shows 2.5-times higher n_S and 1.5-times higher μ_n at room temperature, indicating better transport properties due to lower dislocation density.

Figure 2(a) shows the capacitance–voltage (C–V) characteristics measured on the HEMT diode at 100 kHz. Two distinct regions are observed in reverse bias due to the depletion of the 2DEG and the doped channel. The n_S under the gate contact, obtained by integrating the C–V, is $\sim 1.5 \times 10^{13}\,cm^{-2}$, which agrees with Hall. Figure 2(b) and the inset graph show the doping vs depth as extracted from C–V. These graphs confirm the presence of the 2DEG 18 nm below the barrier's surface and $>10^{17}\,cm^{-3}$ n-type doping in the $Al_{0.6}Ga_{0.4}N$ channel up to 150 nm.

The HEMT output characteristics of each device are compared in Fig. 3(a). For both devices, values are reported for gate-to-source voltage (V_{GS}) from 2 to −4 V with a step of −1 V. The drain to source spacing for device-A and device-B are 7 and 5 μm, respectively. The gate length for both devices is 1.5 μm. For device-A, the maximum drain current ($I_{D,max}$) is 6 mA/mm at $V_{GS} = 2$ V, and the drain saturation current ($I_{D,sat}$) is 2 mA/mm at $V_{GS} = 0$ V. In comparison, for device-B, $I_{D,max}$ is 10 mA/mm at $V_{GS} = 2$ V, and $I_{D,sat}$ is 8 mA/mm at $V_{GS} = 0$ V. It should also be noted that device-A has a large turn-on

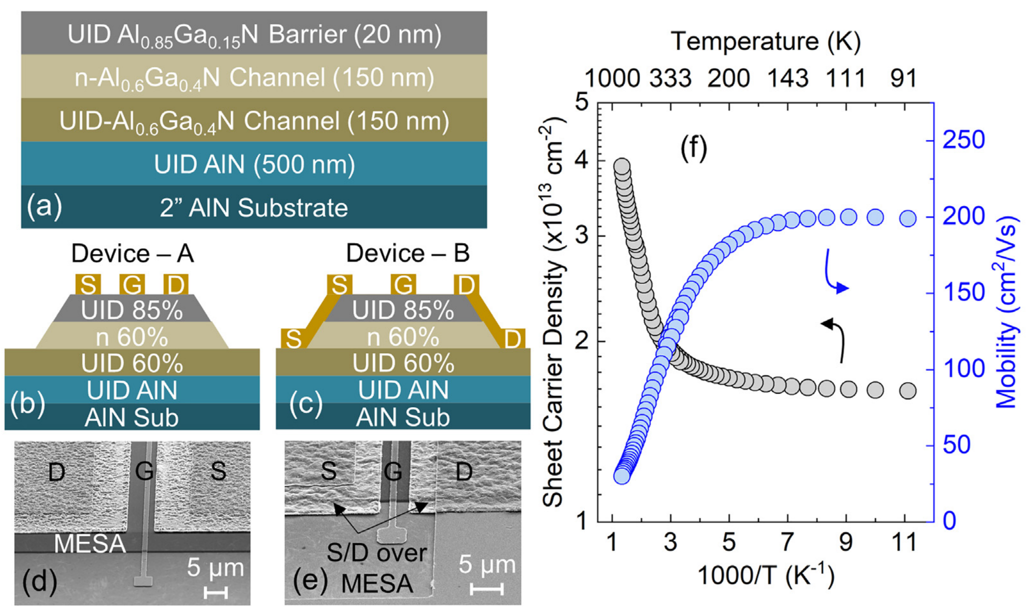

FIG. 1. (a) A schematic cross section of the AlGaN channel HEMT structure grown on a 2-in. AlN substrate. A cross-sectional schematic of fabricated HEMT with source/drain (S/D) contacts (b) on top of mesa only (device-A) and (c) extended over the mesa sidewall (device-B). SEM images of (d) device-A and (e) device-B. (f) Temperature dependent sheet carrier density (n_S) and mobility (μ_n) measured via Hall measurements.

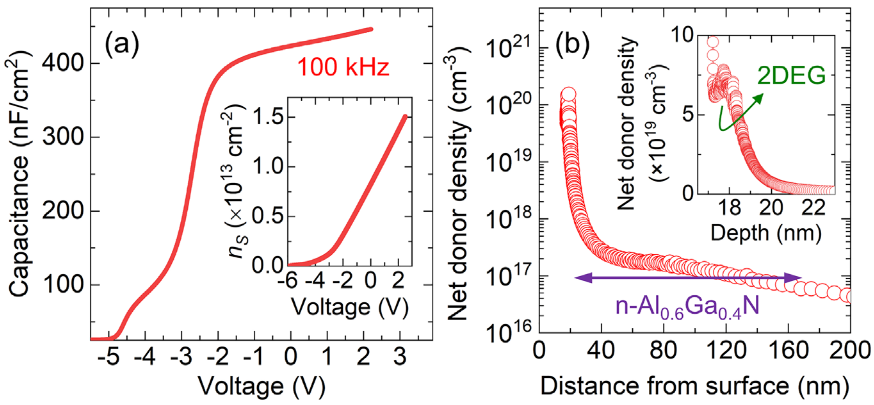

FIG. 2. (a) Capacitance–voltage (C–V) measured on the HEMT Schottky diode at 100 kHz. The inset of (a) shows the sheet carrier density (n_S) as a function of the voltage bias extracted from C–V. (b) The net donor density profile of the HEMT structure extracted from C–V in the semi-log scale. The inset (b) shows the same density profile in the linear scale magnified at the interface between the barrier and the channel layer.

voltage and knee voltage of ~2 V larger than that of device-B. This is attributed to the difference in Ohmic contact design; in the latter case, the contacts are connected to the doped channel layer through the mesa sidewall, which helps reduce the contact resistance. It is, therefore, expected that in device-B, carriers are primarily injected directly into the channel layer from the sidewall when $V_{DS} < 2$ V; above this range, the total current is comprised of both sidewall and topside injection. These mechanisms will be studied more carefully in the future. Compared to GaN HEMTs, the lower mobility and significantly larger contact resistance in AlGaN HEMTs reduce the current density. Nevertheless, the dependence on the contact designs shown in our work shows promise for future performance improvements.

Figure 3(b) shows the transfer characteristics of the HEMT in the linear scale for the device-B geometry measured at drain-source voltage (V_{DS}) = 10 V. The extracted threshold voltage (V_{th}) is −2.9 V, and the maximum transconductance ($g_{m,max}$) is 3.6 mS/mm. Figure 3(c) shows the drain (I_D) and gate (I_G) current on a semi-log plot. When the device is OFF, the drain current leakage is lower than 1 pA/mm, and the gate current also stays in the same current level. The on/off ratio of the HEMT is ~10^{10}, as seen from Fig. 3(c). It should also be noted that no hysteresis was observed.

To better understand the S/D contact behavior, scanning transmission electron microscopy (STEM) was performed. Figure 4(a) shows the STEM of the alloyed metal/$Al_{0.85}Ga_{0.15}N$ barrier/$Al_{0.6}Ga_{0.4}N$ channel/AlN epilayer. The STEM does not show any defects in the epilayers, which confirms the high-quality growth on the native AlN substrate. Figure 4(b) shows the STEM image of the interface between the alloyed metal contact and the $Al_{0.85}Ga_{0.15}N$ barrier layer from the region highlighted in Fig. 4(a). The images show that metals do not penetrate through the barrier layer after alloying the contacts, which might be the reason for poor S/D Ohmic contacts. Limited metal penetration into Al-rich AlGaN has also been reported elsewhere,[18,19] which has prompted studies of various contact metallurgies,[19] regrown contacts,[20] and graded AlGaN layer contacts.[21] These results differ from what is observed in GaN HEMT technology.[22–24]

The two-terminal mesa breakdown characteristics were measured to estimate the electric field strength of the $Al_{0.6}Ga_{0.4}N$ channel layer. Figure 5(a) shows the result for two mesa separations (d): 1.3 and 3.3 μm. These were measured via AFM and defined as the distance between the two UID $Al_{0.6}Ga_{0.4}N$ layers at the base of the mesa etch. The cross-sectional schematic of the mesa separation structure is shown in the inset of Fig. 5(a). The 1.3 μm mesa separation shows breakdown at ~1500 V, which corresponds to a breakdown electric field of 11.5 MV/cm across the UID $Al_{0.6}Ga_{0.4}N$ layer. This is the highest breakdown field measured for Al-rich AlGaN layers.

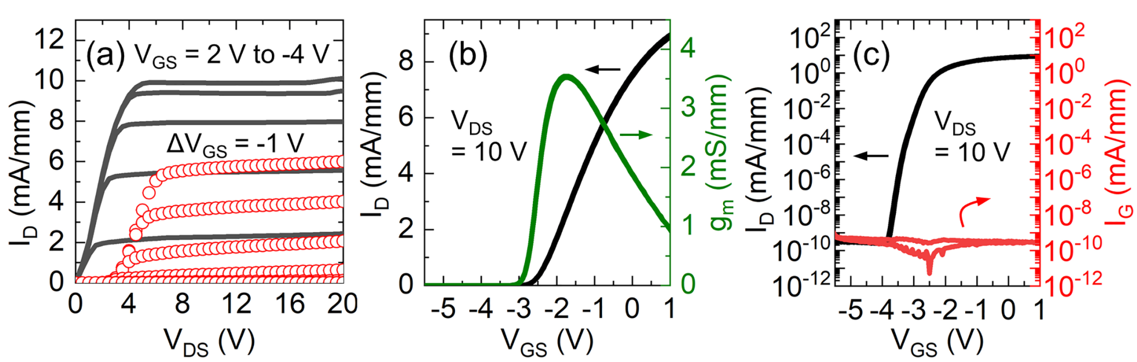

FIG. 3. (a) Output characteristics of device-A (circles) and device-B (lines). Transfer characteristics of device-B in (d) linear- and (e) log-scales.

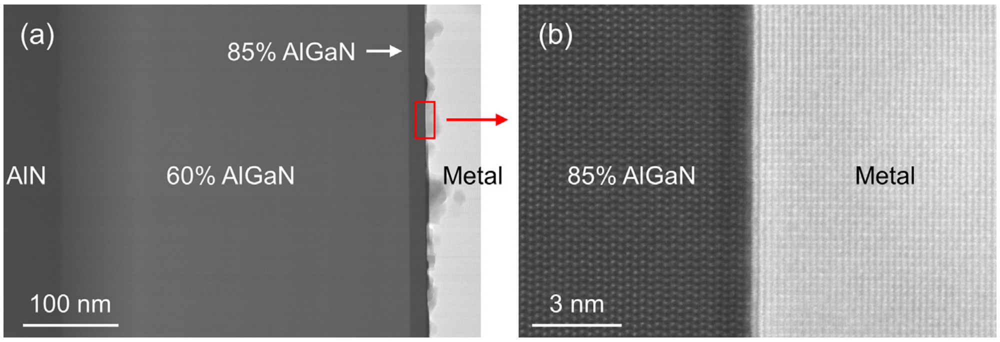

FIG. 4. The cross-sectional STEM images of the (a) alloyed Ohmic metal/$Al_{0.85}Ga_{0.15}N$ barrier/$Al_{0.6}Ga_{0.4}N$ channel/AlN and (b) interface between alloyed metal and $Al_{0.85}Ga_{0.15}N$ barrier layer from the boxed region shown in (a).

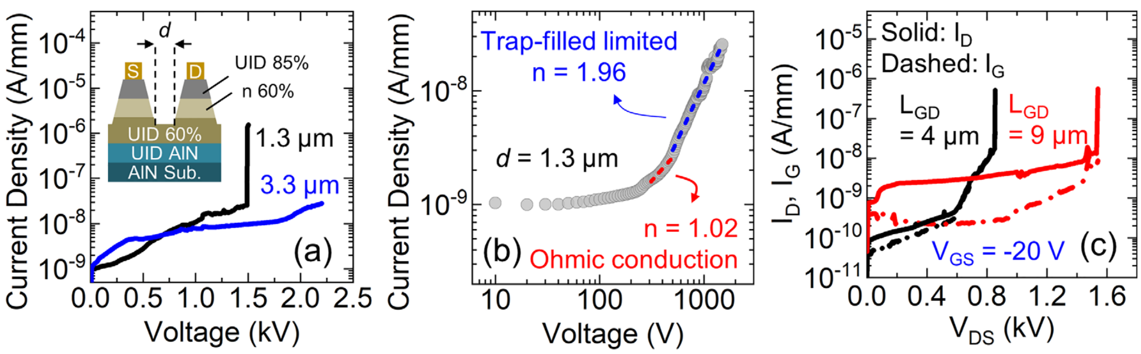

FIG. 5. Two-terminal mesa breakdown for the UID $Al_{0.6}Ga_{0.4}N$ layer. The inset image shows the schematic cross section of the structure. (b) Log(J) vs log(V) characteristics of two-terminal mesa breakdown for 1.3 μm mesa distance. The dashed line shows the fitting for the SCLC model. (c) Three-terminal breakdown characteristics of HEMTs for L_{GD} of 4 and 9 μm. The L_{SG} and L_G are 1.5 μm each and V_{GS} is -20 V.

In comparison, it is ~2× and ~4× higher than the UID AlN buffer mesa breakdown field reported for AlN/$Al_{0.5}Ga_{0.5}N$/AlN HEMTs[11,12] and AlN MESFETs,[25] respectively. The 3.3 μm mesa separation device is measured up to 2200 V as shown in Fig. 5(a) due to the measurement instrument limitation. The device does not break down across this range, indicating that it can sustain an electric field of >6.7 MV/cm. These findings support the conclusion that growth on AlN substrates leads to high-quality epilayers with very low dislocation densities. This is also in agreement with approximately 10 MV/cm breakdown fields observed in the avalanche photodiodes (APDs) grown on AlN substrates.[14,15,26]

To investigate the leakage conduction mechanism in the mesa breakdown structure, the I–V characteristic for a mesa separation of 1.3 μm is analyzed by plotting in the log-log scale, as shown in Fig. 5(b). The leakage does not show an appreciable increase until approximately 300 V. Between 300 V and breakdown at 1.5 kV, the leakage current follows a voltage-dependent power law ($J \propto V^n$). In the 300–500 V regime, the leakage current follows Ohm's law ($n = 1$), implying weak injection from the metal contacts into UID $Al_{0.6}Ga_{0.4}N$ where the trap states are partially filled. Above 500 V, a $J \propto V^2$ (i.e., $n = 2$) dependence is observed, which indicates the onset of space charge limited conduction (SCLC).[27,28] As AlGaN HEMT technology matures, more studies of buffer leakage mechanisms will be pursued.[29]

The three-terminal HEMT breakdown characteristics for two different gate-to-drain (L_{GD}) distances, 4 and 9 μm, are shown in Fig. 5(c). In both cases, the source-to-gate (L_{SG}) distance and gate length (L_G) are 1.5 μm, and V_{GS} is -20 V. As seen, the 4 and 9 μm devices break down at V_{DS} 850 and 1500 V, respectively, without using any edge termination techniques. It should be noted that the off-state current stays below 10 nA/mm for both cases before breakdown. These results are comparable to the reported breakdown values for HEMTs in the literature, even though the channel layer is doped in our case. The estimation of the maximum electric field for these devices requires TCAD simulations, which are left for the future work.

In summary, high-quality $Al_{0.85}Ga_{0.15}N$/$Al_{0.6}Ga_{0.4}N$ HEMT structures were grown on a 2-inch native AlN substrate via MOCVD. We report a breakdown field of ~11.5 MV/cm in the UID $Al_{0.6}Ga_{0.4}N$ layer via mesa isolation structures. This is the largest experimentally observed field in such devices thus far and underlines the promise of UWBG nitrides for extreme electronics.

This work was supported by the NSF (Nos. ECCS-1508854, ECCS-1610992, ECCS-1843395, ECCS-1916800, ECCS-1653383, and DMR-1508191), AFOSR (Nos. FA9550-17-1-0225, FA9550-19-1-0114, and FA9550-19-1-0358), ARO (Nos. W911NF-16-C-0101, W911NF-15-2-0068, and W911NF-18-1-0415), and DOE (No.

DE-SC0011883) and the PowerAmerica Institute at North Carolina State University. S.P. acknowledges the support of NC State University faculty start-up funds. This work was performed in part at the NCSU Nanofabrication Facility (NNF) and Analytical Instrumentation Facility (AIF), which are supported by the State of North Carolina and the National Science Foundation (Award No. ECCS-1542015). The NNF and AIF are members of the North Carolina Research Triangle Nanotechnology Network (RTNN), a site in the National Nanotechnology Coordinated Infrastructure (NNCI).

AUTHOR DECLARATIONS

Conflict of Interest

The authors have no conflicts to disclose.

DATA AVAILABILITY

The data that support the findings of this study are available from the corresponding author upon reasonable request.

REFERENCES

[1] M. A. Khan, Q. Chen, M. S. Shur, B. T. Dermott, J. A. Higgins, J. Burm, W. Schaff, and L. F. Eastman, Electron. Lett. **32**, 357 (1996).
[2] U. K. Mishra, P. Parikh, and Y.-F. Wu, Proc. IEEE **90**, 1022 (2002).
[3] M. Hikita, M. Yanagihara, K. Nakazawa, H. Ueno, Y. Hirose, T. Ueda, Y. Uemoto, T. Tanaka, D. Ueda, and T. Egawa, in *IEEE International Electron Devices Meeting* (IEEE, 2004), pp. 803–806.
[4] E. A. Jones, F. F. Wang, and D. Costinett, IEEE J. Emerg. Sel. Top. Power Electron. **4**, 707 (2016).
[5] J. Y. Tsao, S. Chowdhury, M. A. Hollis, D. Jena, N. M. Johnson, K. A. Jones, R. J. Kaplar, S. Rajan, C. G. Van de Walle, E. Bellotti, C. L. Chua, R. Collazo, M. E. Coltrin, J. A. Cooper, K. R. Evans, S. Graham, T. A. Grotjohn, E. R. Heller, M. Higashiwaki, M. S. Islam, P. W. Juodawlkis, M. A. Khan, A. D. Koehler, J. H. Leach, U. K. Mishra, R. J. Nemanich, R. C. N. Pilawa-Podgurski, J. B. Shealy, Z. Sitar, M. J. Tadjer, A. F. Witulski, M. Wraback, and J. A. Simmons, Adv. Electron. Mater. **4**, 1600501 (2018).
[6] E. Johnson, in *IRE International Convention Record* (IEEE, 1965), pp. 27–34.
[7] B. J. Baliga, IEEE Electron Device Lett. **10**, 455 (1989).
[8] J. L. Hudgins, G. S. Simin, E. Santi, and M. A. Khan, IEEE Trans. Power Electron. **18**, 907 (2003).
[9] A. G. Baca, A. M. Armstrong, B. A. Klein, A. A. Allerman, E. A. Douglas, and R. J. Kaplar, J. Vac. Sci. Technol. A **38**, 020803 (2020).
[10] S. Muhtadi, S. M. Hwang, A. Coleman, F. Asif, G. Simin, M. Chandrashekhar, and A. Khan, IEEE Electron Device Lett. **38**, 914 (2017).
[11] I. Abid, R. Kabouche, F. Medjdoub, S. Besendörfer, E. Meissner, J. Derluyn, S. Degroote, M. Germain, and H. Miyake, in *32nd International Symposium on Power Semiconductor Devices and ICs (ISPSD)* (IEEE, 2020), pp. 310–312.
[12] I. Abid, J. Mehta, Y. Cordier, J. Derluyn, S. Degroote, H. Miyake, and F. Medjdoub, Electronics **10**, 635 (2021).
[13] R. Dalmau and Z. Sitar, in *Springer Handb. Cryst. Growth*, edited by G. Dhanaraj, K. Byrappa, V. Prasad, and M. Dudley (Springer, Berlin/Heidelberg, 2010), pp. 821–843.
[14] P. Reddy, M. Hayden Breckenridge, Q. Guo, A. Klump, D. Khachariya, S. Pavlidis, W. Mecouch, S. Mita, B. Moody, J. Tweedie, R. Kirste, E. Kohn, R. Collazo, and Z. Sitar, Appl. Phys. Lett. **116**, 081101 (2020).
[15] P. Reddy, D. Khachariya, W. Mecouch, M. H. Breckenridge, P. Bagheri, Y. Guan, J. H. Kim, S. Pavlidis, R. Kirste, S. Mita, E. Kohn, R. Collazo, and Z. Sitar, Appl. Phys. Lett. **119**, 182104 (2021).
[16] D. Khachariya, S. Mita, P. Reddy, S. Dangi, P. Bagheri, M. H. Breckenridge, R. Sengupta, E. Kohn, Z. Sitar, R. Collazo, and S. Pavlidis, in Device Research Conference (DRC) (2021).
[17] M. Grundmann, BandEng, see http://My.Ece.Ucsb.Edu/Mgrundmann/Bandeng/ (2005).
[18] N. Yafune, S. Hashimoto, K. Akita, Y. Yamamoto, and M. Kuzuhara, Jpn. J. Appl. Phys., Part 1 **50**, 100202 (2011).
[19] B. A. Klein, A. G. Baca, A. M. Armstrong, A. A. Allerman, C. A. Sanchez, E. A. Douglas, M. H. Crawford, M. A. Miller, P. G. Kotula, T. R. Fortune, and V. M. Abate, ECS J. Solid State Sci. Technol. **6**, S3067 (2017).
[20] E. A. Douglas, S. Reza, C. Sanchez, D. Koleske, A. Allerman, B. Klein, A. M. Armstrong, R. J. Kaplar, and A. G. Baca, Phys. Status Solidi A **214**, 1600842 (2017).
[21] S. Bajaj, F. Akyol, S. Krishnamoorthy, Y. Zhang, and S. Rajan, Appl. Phys. Lett. **109**, 133508 (2016).
[22] A. N. Bright, P. J. Thomas, M. Weyland, D. M. Tricker, C. J. Humphreys, and R. Davies, J. Appl. Phys. **89**, 3143 (2001).
[23] M. W. Fay, G. Moldovan, P. D. Brown, I. Harrison, J. C. Birbeck, B. T. Hughes, M. J. Uren, and T. Martin, J. Appl. Phys. **92**, 94 (2002).
[24] D. Selvanathan, F. M. Mohammed, A. Tesfayesus, and I. Adesida, J. Vac. Sci. Technol. BB. **22**, 2409 (2004).
[25] H. Okumura, S. Suihkonen, J. Lemettinen, A. Uedono, Y. Zhang, D. Piedra, and T. Palacios, Jpn. J. Appl. Phys., Part 1 **57**, 04FR11 (2018).
[26] P. Reddy, W. Mecouch, M. Hayden Breckenridge, D. Khachariya, P. Bagheri, J. Hyun Kim, Y. Guan, S. Mita, B. Moody, J. Tweedie, S. Pavlidis, R. Kirste, E. Kohn, R. Collazo, and Z. Sitar, Phys. Status Solidi RRL 2100619 (2022).
[27] A. Rose, Phys. Rev. **97**, 1538 (1955).
[28] F.-C. Chiu, Adv. Mater. Sci. Eng. **2014**, e578168.
[29] P. Moens, A. Banerjee, M. J. Uren, M. Meneghini, S. Karboyan, I. Chatterjee, P. Vanmeerbeek, M. Cäsar, C. Liu, A. Salih, E. Zanoni, G. Meneghesso, M. Kuball, and M. Tack, in IEEE International Electron Devices Meeting (IEDM) (2015).